American Mineralogist, Volume 88, pages 1697–1702, 2003

Woodruffite: A new Mn oxide structure with 3 × 4 tunnels

JEFFREY E. POST,[1,*] PETER J. HEANEY,[2] CHRISTOPHER L. CAHILL,[3,4] AND LARRY W. FINGER[4]

[1]Department of Mineral Sciences, Smithsonian Institution, Washington, D.C. 20560-0119, U.S.A.
[2]Department of Geosciences, 309 Deike, Pennsylvania State University, University Park, Pennsylvania 16802-2714, U.S.A.
[3]Department of Chemistry, The George Washington University, Washington, D.C. 20052, U.S.A.
[4]Geophysical Laboratory, Carnegie Institution of Washington, Washington, D.C. 20015-1305, U.S.A.

ABSTRACT

The mineral woodruffite, $Zn^{2+}_{x/2}$ $(Mn^{4+}_{1-x}$ $Mn^{3+}_{x})O_2 \cdot yH_2O$, $x \sim 0.4$ and $y \sim 0.7$, is the first known example of a new type of Mn oxide characterized by large tunnels that measure 3 and 4 octahedra (6.9 × 9.2 Å) on a side. These tunnels are rectangular in cross-section and are the largest of any yet reported in natural or synthetic Mn oxides. The thermal stability of woodruffite is comparable to that of todorokite and other large-tunnel Mn oxide phases, breaking down at ~300 °C and eventually transforming to a spinel-type structure. The woodruffite structure may serve as a model for a new class of octahedral molecular sieves with enhanced capabilities as catalysts and selective cation-exchange agents.

INTRODUCTION

Microporous manganese oxide minerals act as important chemical controls in soils and sediments and associated water systems, and with their synthetic analogs they are valued for their catalytic, ion exchange, electrochemical, and adsorption properties (Weis 1968; Nitta 1984; Shen et al. 1993; Kanoh et al. 1997; Dyer et al. 2000). The atomic frameworks of these materials are constructed from Mn-O octahedra that share edges and link corners to yield a panoply of phases with tunnel or layer structures. Of particular interest have been Mn oxide catalysts with large tunnel structures, which are also known as octahedral molecular sieves (OMS). Because these materials exhibit a variety of tunnel shapes and sizes, they offer selectivity for particular species in chemical reactions and the potential for a range of complementary catalytic or cation-exchange applications. Some of the most promising and intensely studied Mn-oxide catalysts are those with the todorokite structure because of their large tunnels and ease of preparation.

Todorokite, until now, held the record for the largest tunnels of any natural or synthetic Mn oxide. In todorokite, triple chains of edge-sharing $Mn^{4+,3+}$-O octahedra share corners to form tunnels with square cross-sections that measure three octahedra on a side (3 × 3). The tunnels in natural samples are partially filled with water molecules and a range of cations, including Mg^{2+}, Ca^{2+}, K^+, Na^+, and Ba^{2+} (Post and Bish 1988). Scientists have developed a variety of methods for synthesizing todorokite-like materials (Shen et al. 1993; Golden et al. 1986; Luo et al. 1999; Nicolas-Tolentino et al. 1999; Vileno et al. 1999), and these synthetic phases have been shown to be effective cathode materials for rechargeable Li batteries (Duncan et al. 1998), selective ion-exchange agents for immobilization of certain metal radionuclides (Kanoh et al. 1997), and highly active oxidative catalysts (Shen et al. 1993; Brock et al. 1998; Vileno et al. 1999). Here we describe a new Mn-oxide structure type with even larger tunnels (3 × 4 octahedral units in cross section, measuring 6.9 × 9.2 Å) than those of todorokite, offering a prototype for a new class of OMS materials.

Woodruffite, zinc manganese oxide hydrate, was first described from oxidized zinc ores of Sterling Hill, NJ (Frondel 1953). At this locality, the samples invariably occur as fine-grained masses, and because their X-ray powder diffraction patterns resemble that produced by todorokite, woodruffite was assumed to be a Zn-rich variety of that mineral. Recently, however, tiny, needle-like crystals of woodruffite were discovered in an oxidized ore body near Mapimi, Durango, Mexico. Although the chemical analyses and XRD pattern for the new crystals corresponded reasonably well with those of woodruffite from Sterling Hill, the diffraction pattern could not be indexed assuming the todorokite structure. In fact, the presence of a 12.4 Å line in the woodruffite XRD patterns, which was not detected on the Debye-Scherrer films in the early work on the poorly crystallized NJ samples, clearly indicated a structure different from that of todorokite. Likewise, selected area electron diffraction (SAED) patterns and high-resolution transmission electron microscopy (HRTEM) images were not consistent with the todorokite 3 × 3 tunnel structure.

The crystals from Mexico measured a few micrometers in cross-section and up to several hundred micrometers in length. Until recently, such crystals would have been too small for single-crystal X-ray diffraction studies, but the new generation of X-ray detectors and high intensity synchrotron X-ray sources now permit structural studies of crystals only a few micrometers in size.

EXPERIMENTAL METHODS

Data collection

The crystal structure of woodruffite was solved using direct methods and single-crystal X-ray diffraction data from a crystal measuring 2.5 × 2.5 × 90 μm. Approximately 1800 reflections were measured with a Bruker *P*4 diffractometer with a Smart 1000 CCD detector using Mo*K*α radiation and 60 s

* E-mail: post.jeffrey@nmnh.si.edu

exposures per 0.3° frames (ω scans). Refinement using these data resulted in a relatively high residual (R = 0.105) with correspondingly large errors on the bond lengths. Subsequently, a low-temperature (123 K) data set was collected from a second crystal measuring 3.0 × 3.0 × 100 μm at the ChemMatCars beamline at the Advanced Photon Source (APS) synchrotron. Here, data were collected on a modified 4-circle diffractometer using a Bruker SMART-6000 CCD detector and a wavelength of 0.5594 Å at a crystal to detector distance of 5.0 cm. Approximately 1250 frames were collected using 0.3° frames (ψ scans) with 2 s exposures. This collection yielded 2069 reflections, of which 724 were independent and observed. Data were corrected for absorption using SADABS to give a final R_{int} of 0.0523. Further details of the collection for the APS experiment are summarized in Table 1.

Electron microprobe analysis of a different crystal from the same sample indicated the following composition: $Zn_{2.8}(Mn^{+4}_{8.4},Mn^{+3}_{5.6})O_{28}\cdot 9.5H_2O$. The proportion of tetra- and trivalent Mn was assigned to balance the charge of the Zn cations in the tunnels, and the water was calculated from Frondel's analysis (Frondel 1953). The Mexican crystals were too small for water analysis, but low microprobe totals and infrared spectra confirmed the presence of a considerable amount of water.

Transmission electron microscopy was performed using crushed grain mounts prepared by grinding woodruffite crystals in ethanol with an agate mortar and pestle and depositing the suspension on a holey C grid. Analyses were obtained with a Philips CM200 FEG-TEM operating at 200 kV equipped with a PGT-IMIX system for energy dispersive X-ray spectroscopy. High-resolution image simulations were performed with the program MacTempas (Total Resolution, Inc.) for the following parameters: voltage = 200 kV; thickness = 60 Å; defocus = –80 nm; C_s = 1.2 mm.

Temperature-resolved X-ray diffraction data were collected at Beamline X7B, National Synchrotron Light Source (NSLS), Brookhaven National Laboratory. Samples in 0.5 mm quartz-glass capillaries were heated at 3 °C/min and the data were obtained using X-ray radiation with wavelength 0.9273 Å and a MAR 345 imaging plate system. The samples were heated using a Blake Instruments furnace with a Pt-13%Rh coiled wire yoke encased in ZrO_2 cement (Brown et al. 1973). The temperature was varied with an Omega controller and monitored with a Chromel-Alumel thermocouple located ~2 mm from the specimen. The actual sample temperature was determined for the range 298 to 1273 K by a variety of melting transitions and by the placement of an additional thermocouple in the sample position. The highly linear relationship between the observed and actual temperatures (r^2 = 0.983) allowed us to calculate a calibration curve with an estimated error of ±5 K for a given temperature. Temperature resolved data from 298 to 1073 K were collected as a series of 120 s exposures. Diffraction patterns were derived from the imaging plate data using full intensity integration of the diffraction rings, as obtained using the program Fit2D (Hammersley et al. 1996) with a polarization factor of 0.93.

Structure solution and refinement

The structure was solved using the Bruker-AXS SHELXTL direct methods package, version 5.10. It consists of triple and quadruple chains of edge-sharing $Mn^{4+,3+}$-O octahedra that link to form large tunnels with rectangular-shaped cross-sections that measure three and four octahedra per side (Fig. 1). Difference-Fourier maps revealed several partially occupied Zn cation and water molecule sites in the tunnels. The structure was refined using the APS data, and the final refinement parameters and residual indices are given in Table 1. The unit-cell parameters are given in Table 2, atom positions and displacement factors are listed in Table 3, and selected bond lengths in Table 4. Anisotropic displacement factors are listed in Table 5[1] and observed and calculated structure factors in Table 6[1].

TABLE 1. Crystal data and structure refinement for woodruffite

Empirical formula	$Zn_{2.8}Mn_{13.8}O_{28}\cdot 9.7H_2O$
Formula weight	1593.25
Temperature	123(2) K
Wavelength	0.55940 Å
Crystal system	monoclinic
Space group	$C2/m$
Z	1
Density (calculated)	3.983 Mg/m^3
Absorption coefficient	4.405 mm^{-1}
F(000)	754
Crystal size	0.003 × 0.003 × 0.10 mm
Theta range for data collection	4.11 to 20.38°
Index ranges	$-28 \le h \le 30$, $-3 \le k \le 3$, $-11 \le l \le 11$
Reflections collected	2069
Independent reflections	724 (R_{int} = 0.0523)
Completeness to θ = 20.21°	87.8%
Refinement method	Full-matrix least-squares on F^2
Data / restraints / parameters	724 / 0 / 82
Goodness-of-fit on F^2	1.087
Final R indices [$I > 2\sigma(I)$]	$R1$ = 0.0694, $wR2$ = 0.1578
R indices (all data)	$R1$ = 0.0866, $wR2$ = 0.1678
Largest diff. peak and hole	2.199 and –1.522 e.Å^{-3}

TABLE 2. Woodruffite unit-cell parameters

Experiment	a (Å)	b (Å)	c (Å)	β (°)	Volume (Å^3)
APS-123 K	24.625(1)	2.8355(1)	9.5381(5)	94.104(2)	664.27(6)
NSLS-100 K	24.765(5)	2.8473(3)	9.559(8)	93.77(1)	672.7(1)
NSLS-298 K	24.810(3)	2.8503(2)	9.581(7)	93.845(5)	676.00(8)

TABLE 3. Atomic coordinates, equivalent isotropic displacement parameters (Å^2), and occupancy factors for woodruffite at 100 K

	x	y	z	U_{eq}*	Occ.
Mn1	0.1998(1)	0	0.142(1)	0.004(1)	1.0
Mn2	0.0920(1)	0.5	0.0059(1)	0.003(1)	1.0
Mn3	0.0094(1)	0	0.2356(1)	0.004(1)	0.940(2)M
Mn4	0	0.5	0.5	0.012(1)	1.0
O1	0.0646(2)	0	0.1117(4)	0.004(1)	1.0
O2	0.2728(2)	0	0.0992(5)	0.006(1)	1.0
O3	0.1766(2)	0.5	0.1236(5)	0.010(1)	1.0
O4	0.0288(2)	0.5	–0.1500(5)	0.008(1)	1.0
O5	0.0454(2)	0.5	0.3498(5)	0.011(1)	1.0
O6	0.1300(2)	0	–0.0819(4)	0.004(1)	1.0
O7	–0.0364(2)	0	0.3991(5)	0.014(1)	1.0
OW1	0.2401(19)	0	0.6170(50)	0.077(14)	0.24(1)
OW2	0.3454(4)	0	0.6153(9)	0.048(2)	0.840(8)O
OW3	0.2619(6)	0	0.3863(17)	0.075(5)	0.64(1)
OW4	0.3621(5)	–0.6840(50)	0.3497(12)	0.062(4)	0.48(1)
Zn1	0.3026(1)	–0.6448(16)	0.4823(2)	0.068(2)	0.330(2)
Zn2	0	0	0	0.002†	0.085(1)

* U_{eq} is defined as one third of the trace of the orthogonalized U_{ij} tensor.
† The isotropic atomic displacement factor for Zn2 was fixed.

TABLE 4. Selected woodruffite bond distances (Å)

Mn1-O2 (×2)	1.934(3)	Mn3-O1	1.866(4)
Mn1-O2	1.918(4)	Mn3-O4 (×2)	1.857(3)
Mn1-O3 (×2)	1.874(3)	Mn3-O5 (×2)	1.961(3)
Mn1-O6	1.890(4)	Mn3-O7	1.988(5)
<Mn1-O>	1.904	<Mn3-O>	1.915
Mn2-O1 (×2)	1.892(3)	Mn4-O5 (×2)	1.880(5)
Mn2-O3	2.293(5)	Mn4-O7 (×4)	1.902(3)
Mn2-O4	2.075(5)	<Mn4–O>	1.895
Mn2-O6 (×2)	1.922(3)		
<Mn2-O>	1.999		
Zn1-OW2	1.882(8)		
Zn1-OW3	2.13(2)		
Zn1-OW3	2.25(1)		
Zn1-OW4	2.01(1)		
<Zn1-OW>	2.07		

[1]For a copy of Tables 5 and 6, document item AM-03-041, contact the Business Office of the Mineralogical Society of America (see inside front cover of recent issue) for price information. Deposit items may also be available on the American Mineralogist web site at http://www.minsocam.org.

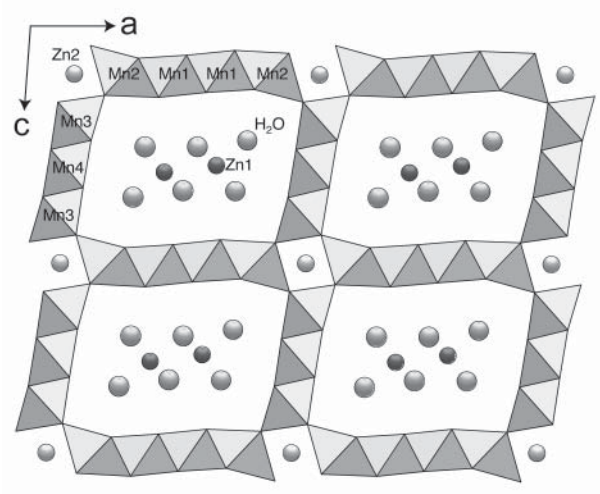

FIGURE 1. Polyhedral representation of the structure of woodruffite viewed along **b**.

The unit-cell parameters refined from the 123 K APS data set (Table 2) were determined by an unconstrained refinement of 1082 reflections (0.8–6.1 Å), and subsequently were constrained to a monoclinic cell. For comparison, the unit-cell parameters determined by Rietveld refinement from powder X-ray diffraction data collected at 298 and ~100 K at NSLS are included in Table 2. The NSLS data were calibrated against a LaB_6 standard. Obviously, the unit-cell parameters for the 123 K APS data are significantly smaller than the comparable NSLS values. The reason for the differences is not known, but based on the results of refinements of unit cells for several standard materials we conclude that the NSLS values are probably more accurate. For consistency, however, the bond distances in Table 4 were calculated using the APS unit-cell parameters.

DISCUSSION

Woodruffite is the first known framework structure constructed of triple and quadruple chains of Mn-O octahedra. The large tunnels have rectangular-shaped cross-sections that measure three by four octahedra, and they are filled by Zn cations and water molecules (Fig. 1).

Octahedral framework

The Mn-O octahedral distances in woodruffite (Table 4) are similar to those reported for the related structures todorokite (Post and Bish 1988) and romanechite (Turner and Post 1988). The average Mn-O distance of 1.93 Å is significantly larger than that of 1.89 Å for pyrolusite (Bauer 1976), indicating that while most of the Mn is tetravalent, some larger, lower valence Mn is also present on the octahedral sites. As a pure MnO_2 framework is charge neutral, the charges of the Zn cations in the tunnels are balanced by the lower valence Mn. The longer average Mn-O bond lengths for the Mn2 sites, which occur at the edges of the quadruple chains, suggest that these sites preferentially accommodate the lower-valence cations. This behavior is consistent with structures reported for romanechite (Turner and Post 1988), todorokite (Post and Bish 1988), a 2×5 Mn oxide tunnel structure (Tamada and Yamamoto 1986), and a 2×4 Mn oxide tunnel structure (Rziha et al. 1996), which also show larger octahedral sites at the edges of the largest-width chains. These larger sites in woodruffite show elongated axial Mn-O bond lengths (2.29 and 2.08 Å) relative to the equatorial distances (1.92 and 1.89 Å), a characteristic Jahn-Teller distortion indicating that the lower-valence Mn is trivalent. The mean observed Mn1-O distance of 1.999 Å is not significantly different than the expected Mn^{3+}-O bond length of 2.005 Å calculated using the ionic radii of Shannon (1976), suggesting that the Mn2 site is fully occupied by Mn^{3+}. The above chemical formula with 5.6 Mn^{3+} cations per unit cell, required to offset the charges on the 2.8 Zn^{2+} cations in the tunnels, indicates that even with the Mn2 sites completely filled by Mn^{3+}, some trivalent Mn must reside at other Mn sites, most likely Mn3, which is located at the edges of the triple chains and also shows some evidence of octahedral Jahn-Teller-type distortion (Table 4). Assuming only Mn^{3+} and Mn^{4+} cations on the octahedral sites, the average Mn oxidation state for woodruffite is +3.6, which is similar to the value of +3.73 reported by McKeown and Post (2001) for todorokite.

The Mn cations are displaced off center in the octahedra, probably due to cation-cation repulsions between adjacent octahedra. Similar displacements have been reported in hollandite (Post et al. 1982) and romanechite (Turner and Post 1988).

3×4 Tunnel sites

The Zn cations are distributed over two parallel rows of sites near the centers of the 3×4 tunnels (Fig. 1). The Zn sites are about two-thirds filled. The weak rows of superstructure reflections and streaks in the SAED patterns, discussed below, suggest some type of cation-vacancy ordering along and among the tunnels. Difference-Fourier maps show several concentrations of electron density near the Zn cations, and we interpret these as partially occupied water sites. The water positions are about 1.88–2.25 Å from the Zn cations in a distorted tetrahedral coordination. The mean Zn-H_2O distance of 2.07 Å is in reasonable agreement with other reported Zn-H_2O distances (Post and Appleman 1988). Such a tetrahedral arrangement is consistent with the nearly 4:1 ratio of water molecules to Zn cations determined from the chemical analyses and the refined occupancy factors for the water sites (Table 3). The OW1 position is not coordinated to the Zn cation, and is less than 25% occupied. It is possible that OW1 is a water position that is partially occupied when the Zn cation site for a particular unit cell is vacant.

The chemical analyses and structure refinement indicate that ~2/3 of the Zn tunnel sites are filled. This level of occupancy suggests an ordering scheme in a given column of Zn cations with every third tunnel site vacant. Such an arrangement allows the Zn cations to increase their separation distance along a tunnel by displacing away from one another toward their respective adjacent vacancies. This movement increases the Zn-Zn separation from 2.85 to ~3.65 Å, thereby reducing the Zn-Zn repulsion. These displacements are consistent with the split Zn site, with a separation of 0.8 Å, determined by our refinement. A similar splitting has been reported for the Pb cation site in

coronadite (Post and Bish 1989) and the tunnel Cl anion position in akaganéite (Post et al. 2003b). In both coronadite and akaganéite, the tunnel sites are two-thirds filled, as in woodruffite. The observed splitting of the OW4 site, and the large displacement factors for the other water sites, are likely a consequence of the Zn cation displacements. The water positions in a given cell correlate with the position of the local Zn cation.

The electron density maps suggest that the tunnel sites show positional disorder, both within and perpendicular to the mirror planes. Consequently, the refinements yield only average positions, and therefore average bond lengths, that might deviate significantly from actual atomic distances. In addition to the displacements described above the Zn cation and H_2O molecule positions likely are also affected by the local arrangements of Mn^{3+} framework cations (Post and Burnham 1986). The electron scattering represented by the sum of the refined occupancy factors for the tunnel sites identified in our study closely matches the total value determined by chemical analyses, suggesting that all of the significant tunnel sites have been identified.

1 × 1 tunnel cation site

The difference-Fourier maps showed a small, but distinct, electron density peak at (0,0,0) in the centers of the small 1 × 1 tunnels that parallel the 3 × 4 tunnels (Fig. 1). This peak is surrounded by six O atoms in a distorted octahedral coordination, at distances of 1.85 Å (×2) and 2.17 Å (×4). The mean distance of 2.06 Å suggests that a cation, rather than water, must occupy this site, and the value is close to the Zn-O octahedral distance of 2.11 Å predicted using the ionic radii of Shannon (1976). Our refinement yielded an occupancy factor of 0.08, or 0.16 Zn cations per unit cell. A problem with Zn cations at this position, however, is that they are only ~2.24 Å from the Mn3 cations in the neighboring octahedron, an unlikely close distance. Repulsion between Zn and Mn cations is averted if adjacent Mn3 sites are vacant whenever a Zn cation occupies the (0,0,0) position. In fact, our refinement of the occupancy factor for Mn3 yielded a value of 0.95, corresponding to a deficiency of ~0.2 Mn cations per unit cell, close to the number required to accommodate the additional Zn cations. Moreover, the sum of the number of presumed Zn cations in the 1 × 1 tunnels (0.16) and the number of Zn cations refined for the 3 × 4 tunnels (2.64) is equal to the value of 2.80 calculated from the microprobe analysis. It is interesting to note that Duncan et al. (1998) postulated that Li partially occupies the 1 × 1 tunnel in Li-bearing todorokite.

Woodruffite microstructure

High-resolution transmission electron microscope (HRTEM) images of natural todorokite samples show disordered intergrowths of 3 × 4 and even larger tunnels within the predominant 3 × 3 framework (Chukhrov et al. 1978; Turner and Buseck 1981). Nevertheless, woodruffite is the first, and thus far, only macroscopic example of an Mn oxide with 3 × 4 tunnels. Selected area electron diffraction (SAED) patterns and HRTEM images of the Mexican woodruffite crystals reveal a remarkably high degree of order with respect to tunnel size, especially in comparison with the extensively disordered natural and synthetic todorokite samples. No streaking was observed in SAED patterns along [010] (Fig. 2), and lower magnification HRTEM images exhibited regular periodicities over length scales exceeding 100 nm (Fig. 3). Lattice fringes were interrupted only by incipient cleavage along (101), possibly induced during sample preparation of the crushed grain mounts.

On the other hand, diffraction patterns with zone axes normal to **b*** indicated some departures from the idealized structure (Figs. 4 and 5). For example, in acicular crystals (~15 by ~1 μm) elongate along **b**, superlattice diffractions parallel to **b*** were apparent in both [100] and [001] SAED patterns. These patterns reveal a superstructure along the tunnel direction that is eight times the dimension of the primary unit cell, produced perhaps during spiral growth of the whisker-like crystal. In

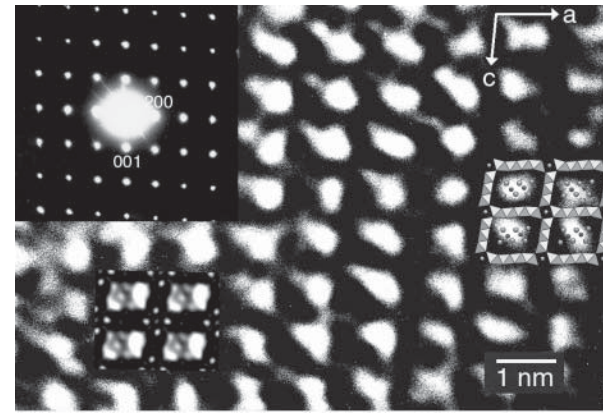

FIGURE 2. HRTEM image and SAED pattern of woodruffite along **b**. An HRTEM simulation of the woodruffite structure (inset left) was generated assuming half-occupancy of the Zn cations in a triclinic cell. A projection along **b** of the refined structure also is superimposed (inset right).

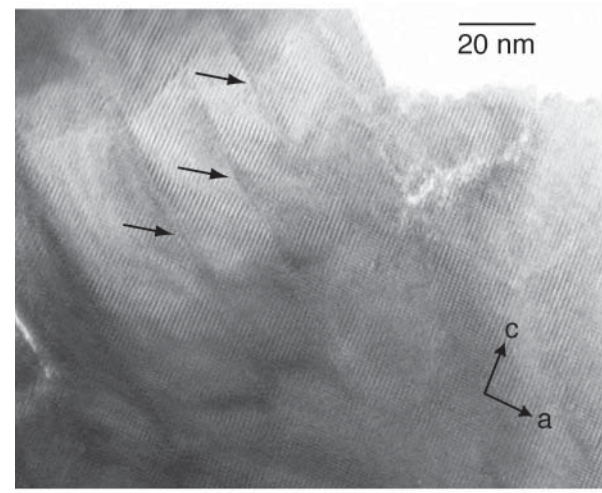

FIGURE 3. An HRTEM image with the [010] zone axis at slightly lower magnification reveals long-range structural uniformity. Cleavage planes along (101) are arrowed.

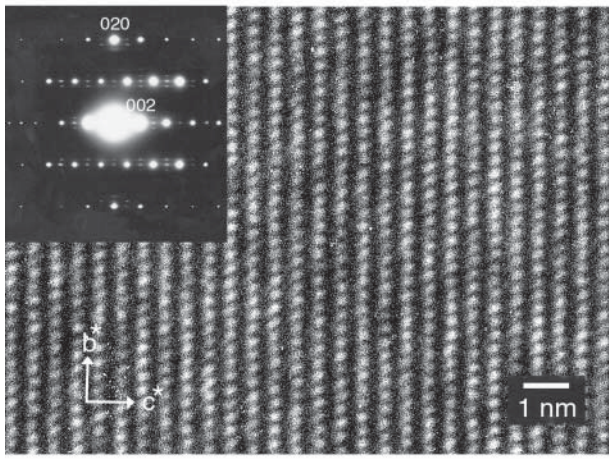

FIGURE 4. HRTEM image and SAED pattern of woodruffite along **a**.

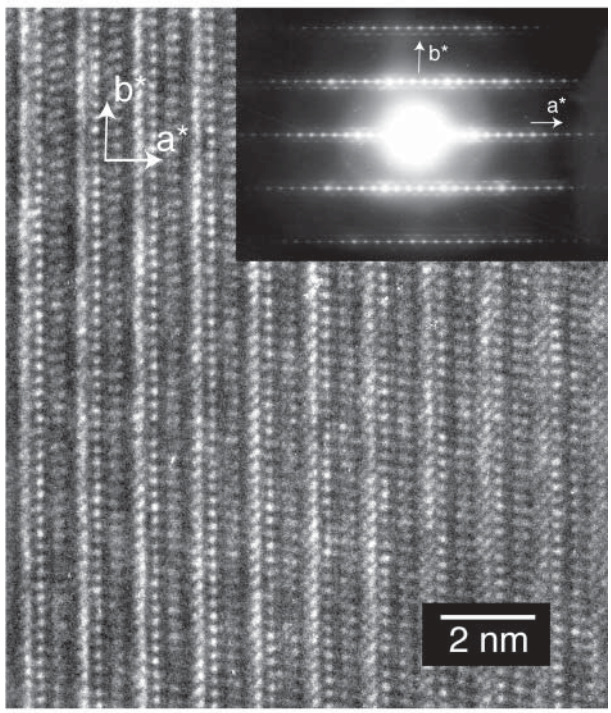

FIGURE 5. HRTEM image and SAED pattern of woodruffite along **c**.

addition, faint streaking along the **a*** and the **c*** directions suggests the presence of short-range ordering among the water molecules and the Zn cations in neighboring tunnels. Lastly, measurements of the SAED patterns produced by the acicular crystal revealed that α^* was 90°, as expected for a monoclinic mineral, but **a*** and **b*** were distinctly non-orthogonal, with a measured value for γ^* of 88.8° (with an estimated error of ±0.2°). Efforts to refine the woodruffite structure in the triclinic space group $C\bar{1}$ ($P\bar{1}$) using single-crystal and powder synchrotron X-ray diffraction data consistently yielded a monoclinic cell. These results imply that the bulk structure of woodruffite conforms to space group symmetry $C2/m$, but that

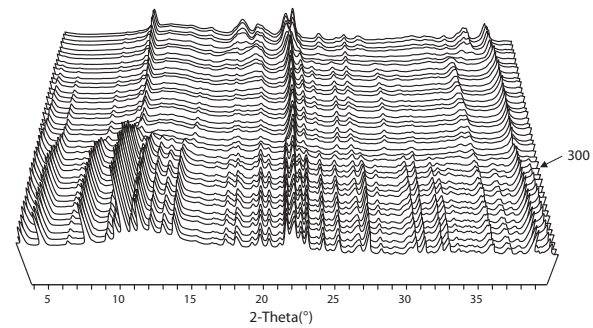

FIGURE 6. Series of powder X-ray diffraction patterns collected as woodruffite was heated from room temperature to 500 °C. The structure starts to break down at approximately 300 °C and eventually transforms to a hausmannite-like phase. The patterns are plotted as intensity vs. degrees 2θ.

local variations in the contents of the tunnels can lead to structural distortions that depart from monoclinicity.

Thermal behavior of woodruffite

In situ powder X-ray diffraction data collected for woodruffite (Fig. 6) and todorokite samples heated from room temperature to 800 °C show that despite having larger tunnels, woodruffite is as thermally stable as todorokite. Structures for both phases begin to break down at approximately 300 °C (Post et al. 2003a). The collapse of both structures is triggered by the loss of O atoms from the octahedral frameworks and the consequent reduction of Mn (Post et al. 2003a), eventually leading to the formation of a hausmannite-like phase. This mechanism suggests that a strategy for preparing more thermally stable todorokite- and woodruffite-like compounds should focus on altering the framework, rather than the tunnel, composition, perhaps substituting cations with less variation in valence state, e.g., Cu^{2+}, Ni^{2+}, and Ti^{4+}, for some of the Mn cations.

ACKNOWLEDGMENTS

We thank J. Hanson for his assistance with the synchrotron X-ray powder diffraction study. J.E.P. acknowledges support from the Smithsonian Institution Sprague Fund, and P.J.H. and S.E.P. acknowledge NSF Grant EAR01-25908 and a grant from the PSU Center for Environmental Chemistry and Geochemistry. CLC acknowledges GWU start-up funding. P. Megaw generously donated one of the woodruffite specimens used in this study. Powder diffraction experiments were performed at the Brookhaven National Laboratory, which is supported under contract DE-AC02-98CH10886 with the U.S. Department of Energy by its Division of Chemical Sciences, Office of Basic Energy Research. We are grateful to V.G. Young, Jr. for his assistance with the single crystal diffraction experiments at the APS. ChemMatCARS Sector 15 is principally supported by the National Science Foundation/Department of Energy under grant number CHE0087817 and by the Illinois Board of Higher Education. The Advanced Photon Source is supported by the U.S. Department of Energy, Basic Energy Sciences, Office of Science, under Contract No. W-31-109-Eng-38.

REFERENCES CITED

Bauer, W.H. (1976) Rutile-type compounds. V. Refinement of MnO_2 and MgF_2. Acta Crystallographica, B32, 2200–2204.

Brock, S.L., Duan, N., Tian, Z.R., Giraldo, O., Zhou, H., and Suib, S.L. (1998) A review of porous manganese oxide materials. Chemistry of Materials, 10, 2619–2628.

Brown, G.E., Sueno, S., and Prewitt, C.T. (1973) A new single-crystal heater for the precession camera and four-circle diffractometer. American Mineralogist, 58, 698–704.

Chukhrov, F.V., Gorshkov, A.I., Sivtsov, A.V., and Beresovskaya, V.V. (1978) Structural varieties of todorokite, Izvestia Akademia Nauk, SSSR, Series Geology

12, 86.
Duncan, M.J., Leroux, F., Corbett, J.M., and Nazar, L.F. (1998) Todorokites as a Li insertion cathode. Journal of the Electrochemical Society, 145, 3746–3757.
Dyer, A., Pillinger, M., Newton, J., Harjula, R., Möller, T., and Amin, S. (2000) Sorption behavior of radionuclides on crystalline synthetic tunnel manganese oxides. Chemistry of Materials, 12, 3798–3804.
Frondel, C. (1953) New manganese oxides; hydrohausmannite and woodruffite. American Mineralogist, 38, 761–769.
Golden, D.C., Chen, C.C., and Dixon, J.B. (1986) Synthesis of todorokite. Science, 231, 717–719.
Hammersley, A.P., Svensson, S.O., Hanflan‹, M., Fitch, A.N., and Hausermann, D. (1996) Two-dimensional detector software: From real detector to idealised image or two-theta scan. High Pressure Research, 14, 235–248.
Kanoh, H., Tang, W., Makita, Y., and Ooi, K. (1997) Electrochemical intercalation of alkali-metal ions into birnessite-type manganese oxide in aqueous solution. Langmuir, 13, 6845–6849.
Luo, J., Zhang, Q., Huang, A., Giraldo, O., and Suib, S.L. (1999) Double-aging method for preparation of stabilized Na-buserite and transformation to todorokites incorporated with various metals. Inorganic Chemistry, 38, 6106–6113.
McKeown, D.A. and Post, J.E. (2001) Characterization of manganese oxide mineralogy in rock varnish and dendrites using X-ray absorption spectroscopy. American Mineralogist, 86, 701–713.
Nicolas-Tolentino, E., Tian, Z.R., Zhou, H., Xia, G., and Suib, S.L. (1999) Effects of Cu^{2+} ions on the structure and reactivity of todorokite- and cryptomelane-type manganese oxide octahedral molecular sieves. Chemistry of Materials, 11, 1733–1741.
Nitta, M. (1984) Characterization of manganese nodules as adsorbents and catalysts, a review. Applied Catalysis, 9, 151–176.
Post, J.E. and Appleman, D.E. (1988) Chalcophanite, $ZnMn_3O_7◊3H_2O$: new crystal structure determination. American Mineralogist, 73, 1401–1404.
Post, J.E. and Bish, D.L. (1988) Rietveld refinement of the todorokite structure. American Mineralogist, 73, 861–869.
——— (1989) Rietveld refinement of the coronadite structure. American Mineralogist, 74, 913–917.
Post, J.E. and Burnham, C.W. (1986) Modeling tunnel-cation displacements in hollandites using structure-energy calculations. American Mineralogist, 71, 1178–1185.
Post, J.E., Von Dreele, R.B., and Buseck, P.R. (1982) Symmetry and cation displacements in hollandites: structure refinements of hollandite, cryptomelane, and priderite. Acta Crystallographica, B38, 1056–1065.
Post, J.E., Heaney, P.J., and Hanson, J. (2003a) Real-time synchrotron X-ray powder diffraction studies of the structure and dehydration of todorokite. American Mineralogist, 88, 142–150.
Post, J.E., Heaney, P.J., Von Dreel, R.B., and Hanson, J. (2003b) Neutron and temperature-resolved sychrotron X-ray powder diffraction study of akaganéite. American Mineralogist, 88, 782–788.
Rziha, T., Gies, H., and Rius, J. (1996) RUB-7 a new synthetic manganese oxide structure type with a 2x4 tunnel. European Journal of Mineralogy, 8, 675–686.
Shannon, R.D. (1976) Revised effective ionic radii and systematic studies of interatomic distances in halides and chalcogenides. Acta Crystallographica, A32, 751–767.
Shen, Y.F., Zerger, R.P., DeGuzman, R.N., Suib, S.L., McCurdy, L., Potter, D.I., and O'Young, C.L. (1993) Manganese oxide octahedral molecular sieves: preparation, characterization, and applications. Science, 260, 511–515.
Tamada, O. and Yamamoto, N. (1986) The crystal structure of a new manganese dioxide ($Rb_{0.27}MnO_2$) with a giant tunnel. Mineralogical Journal, 13, 130–140.
Turner, S. and Buseck, P. R. (1981) Todorokites: a new family of naturally occurring manganese oxides. Science, 212, 1024–1027.
Turner, S. and Post, J.E. (1988) Refinement of the substructure and superstructure of romanechite. American Mineralogist, 73, 1155–1161.
Vileno, E., Zhou, H., Zhang, Q., Suib, S.L., Corbin, D.R., and Koch, T.A. (1999) Synthetic todorokite produced by microwave heating: an active oxidation catalyst. Journal of Catalysis, 187, 285–297.
Weis, P.B. (1968) Deep sea manganese nodules as oxidative catalysts. Journal of Catalysis, 10, 407–412.

MANUSCRIPT RECEIVED OCTOBER 24, 2002
MANUSCRIPT ACCEPTED APRIL 25, 2003
MANUSCRIPT HANDLED BY PETER BURNS